The Child With Macrocephaly: Differential Diagnosis and Neuroimaging Findings

Emanuele Orrù[1]
Sonia F. Calloni[2]
Aylin Tekes[3]
Thierry A. G. M. Huisman[3]
Bruno P. Soares[3]

OBJECTIVE. The purpose of this article is to offer a systematic approach to the imaging of children with macrocephaly and to illustrate key neuroimaging features of common and rare but important disorders.

CONCLUSION. Macrocephaly is a common clinical finding in children. Increased volume of one of the intracranial compartments can enlarge the head either prenatally or postnatally while the cranial sutures are open. Imaging plays a central role in establishing a diagnosis and guiding management.

Keywords: children, CT, hydrocephalus, macrocephaly, megalencephaly, MRI, pediatric

doi.org/10.2214/AJR.17.18693

Received June 29, 2017; accepted after revision August 21, 2017.

[1]Russell H. Morgan Department of Radiology and Radiological Science, Johns Hopkins University School of Medicine, Baltimore, MD.

[2]Università degli Studi di Milano, Postgraduation School in Radiodiagnostics, Milan, Italy.

[3]Russell H. Morgan Department of Radiology and Radiological Science, Division of Pediatric Radiology and Pediatric Neuroradiology, Johns Hopkins University School of Medicine, The Johns Hopkins Hospital, 1800 Orleans St, Zayed Tower, Rm 4174, Baltimore, MD 21287. Address correspondence to B. P. Soares (bruno.soares@jhmi.edu).

AJR 2018; 210:1–12

0361–803X/18/2104–1

Macrocephaly is a commonly encountered entity in pediatric clinical practice, particularly in infants. It is defined as an occipitofrontal circumference greater than 2 SD, or 0.5 cm above the 97th percentile. The occipitofrontal circumference extends from the most prominent part of the glabella to the most prominent posterior area of the occiput [1].

The head is a system composed of a container and its contents, the container being the skull and the contents being the brain, CSF, and blood vessels. After closure of the intracranial sutures, the head becomes a closed system in which the three components of the contents are in a dynamic volumetric equilibrium defined by the Monro-Kellie doctrine, in which it is assumed that within an intact skull, the sum of the volumes of the brain, CSF, and intracranial blood is constant. To keep the intracranial volume balanced, an increase in the size of one component causes a reduction in one or both of the other two [2].

The major cranial sutures normally remain patent beyond early childhood. The exception is the metopic suture, which typically closes in the first year of life [3]. The fontanelles also contribute to head growth and skull compliance. The posterior fontanelle generally closes 2 months after birth, and the anterior fontanelle by 2 years of age in almost all infants [4]. Young children with open sutures therefore constitute a unique population that can accommodate intracranial volumetric increases by expanding the skull. However, as the child grows, the skull becomes less compliant to volumetric changes, and increased intracranial pressure may lead to one of the typical brain herniation syndromes, potentially with severe clinical consequences.

A great number of disorders can affect the brain parenchyma, the intraventricular and extraventricular CSF spaces, and the intracranial blood pool, making the clinical finding of macrocephaly highly nonspecific. Furthermore, a large occipitofrontal circumference can also be secondary to an increased skull thickness with normal intracranial contents. Macrocephaly resulting from an abnormal increase in size of the brain parenchyma is defined as megalencephaly [5].

Macrocephaly is a nonspecific clinical finding without implications about the underlying cause. Therefore, imaging has a key role in clarifying the anatomy and quality of the abnormality causing the increased head circumference. The purposes of this review is to present a systematic approach to neuroimaging of a child with a large head and to illustrate the most commonly encountered and recognizable causes of macrocephaly. Although in clinical practice mechanisms and disorders that cause macrocephaly may overlap, for this article we classify entities by the most prominently enlarged cranial component: extraaxial spaces, ventricles, brain parenchyma, and skull (Table 1).

Approach to Imaging of a Child With a Large Head

Imaging of children is particularly challenging because of their occasional inability

TABLE 1: Causes of Macrocephaly by Enlarged Head Compartment

Enlarged Compartment	Most Relevant Disorders	Key Radiologic Features
Extraaxial spaces	Benign enlargement of subarachnoid spaces	Enlarged anterior subarachnoid spaces with crossing veins and no mass effect
	Hematoma	Subdural collections displace the subarachnoid veins toward the parenchyma; bridging vein thrombosis, parenchymal injury, fractures, retinal hemorrhage
	Glutaric aciduria type 1	Enlarged sylvian fissures with or without basal ganglia signal-intensity abnormalities; can be associated with subdural hemorrhage
Ventricles (hydrocephalus)	Aqueductal stenosis	Supratentorial ventricular dilatation that can be seen prenatally; use of cisternographic sequences can clarify anatomy
Congenital	Chiari II malformation	Small posterior fossa with cerebellar herniation and supratentorial hydrocephalus; associated myelomeningocele
Acquired	Dandy-Walker malformation	Large posterior fossa, cystic dilatation of fourth ventricle, severe hypoplasia and upward rotation of cerebellar vermis
	Posthemorrhagic and infectious disorders	May be associated with extensive periventricular gliosis or leukomalacia
Increased CSF	Postinfectious disorders	May show postinflammatory meningeal thickening
	Midline tumors	ADC values and presence of calcifications narrow the differential diagnosis
	Posterior fossa tumors	ADC values, location, and extension pattern narrow the differential diagnosis
	Choroid plexus tumors	Marked hydrocephalus, usually in the ventricle atrium
Parenchyma (megalencephaly)	Hemimegalencephaly	Dysplasia and enlargement of one hemisphere or part of it
Developmental	Alexander disease	Diffuse progressive white matter abnormalities, predominantly frontal; striatal involvement
Metabolic	Canavan disease	Subcortical white matter and deep gray nuclei involvement, *N*-acetylaspartate peak at spectroscopy.
	Megalencephalic leukoencephalopathy with subcortical cysts	Diffuse swelling and abnormal signal intensity of white matter, subcortical cysts in temporal poles and frontal lobes
	Vanishing white matter disease	Diffuse T2 hyperintensity of white matter with progressive cystic degeneration, residual glial strands
Skull	Achondroplasia	Large cranium with frontal bossing and nasion depression, small foramen magnum; hydrocephalus may also be present
	Thalassemia major	Marked diploic space thickening with "hair on end" appearance of the skull on radiographs

Note—ADC = apparent diffusion coefficient.

to cooperate and the need to establish an accurate diagnosis while limiting radiation exposure to a reasonable minimum [6].

Head ultrasound can be performed while the fontanelles are still open and has excellent spatial and anatomic resolution, particularly within the first 2 months of life. After 6 months, smaller acoustic windows due to closing sutures limit the sensitivity of the examination [7]. CT has excellent spatial resolution and is the best modality for quickly assessing osseous anatomy. In the setting of trauma, it has high sensitivity and specificity for depicting blood products and fractures. Because of rapid acquisition times, it usually does not require sedation. MRI is a nonionizing technique with the highest contrast resolution, but it requires potentially long acquisition times and the possible use of sedation; hence, it is not suitable for every clinical scenario. The use of ultrafast single-shot contiguous T2-weighted sequences has partially obviated this issue. The main advantage of MRI lies in the multitude of sequences that can help clarify specific diagnostic questions. For instance, DW images can show areas of acute infarction or hypercellularity, susceptibility-weighted images can show blood products, and high-resolution cisternographic sequences (e.g., fast imaging employing steady-state acquisition [FIESTA]) allow evaluation of CSF spaces in exquisite anatomic detail, a feature particularly useful for differentiating causes of hydrocephalus. Black bone (ultrashort TE) MRI can help determine the site and anatomic configuration of a fracture. Appropriately encoded phase contrast images allow visualization of normal biphasic flow and facilitate quantitative assessment of CSF flow [8].

A reasonable diagnostic approach to macrocephaly includes performing head ultrasound as the initial screening tool for infants with open fontanelles, obtaining normal findings of a neurodevelopmental examination, and finding no signs concerning for increased intracranial pressure. If ultrasound findings are abnormal, either head CT or brain MRI can be performed. In the acute phase, CT has usually been the mainstay modality because of its rapid acquisition and widespread availability. If MRI is available, quick evaluation of ventricular caliber and intracranial anatomy can be performed without sedation with ultrafast T2-weighted sequences. Sedation or general anesthesia is usually needed for a full diagnostic brain MRI examination that includes high-resolution or volumetric sequences.

Approach to Macrocephaly by Compartments

Enlarged Extraaxial Spaces

Benign enlargement of subarachnoid spaces—Benign enlargement of subarachnoid spaces is the most common cause of macrocephaly in infants, the prevalence being as high as 75% [9, 10]. Children usually present as outpatients with a large head and normal to minimally delayed cognitive development [11]. The condition usually plateaus and resolves spontaneously by 2 years of age. The cause may involve immature or impaired reabsorption of CSF at the arachnoid granulations [12].

Imaging shows symmetric enlargement of the subarachnoid spaces along the frontoparietal convexities and widening of the interhemispheric sulcus. Mild supratentorial ventriculomegaly may also be present. Bridging veins crossing the subarachnoid space are seen as elongated, nonstretched flow voids on T2-weighted images (Fig. 1A). The veins can also be visualized with Doppler ultrasound. Benign enlargement of subarachnoid spaces has been variably associated with a propensity to isolated subdural hemorrhage (SDH), although without definitive proof [13]. An isolated SDH in a child with macrocephaly without other stigmata of abusive head trauma (AHT) suggests a posttraumatic state but should not necessarily lead to a presumptive diagnosis of child abuse [14]. At CT, differentiating subarachnoid space enlargement from subdural collections can be difficult, and the diagnosis of benign enlargement of subarachnoid spaces should be entertained with caution in any child presenting to the emergency department. Finally, the finding of prominent subarachnoid spaces and ventricles in a child with microcephaly, or even a normal-sized head, should raise concern of permanent or transient brain parenchymal volume loss as opposed to benign enlargement of subarachnoid spaces.

Abusive head trauma—AHT usually occurs during the first year of life and is an important cause of long-term morbidity and mortality in children [15]. Pediatric victims of AHT often but not always present in the acute phase of injury. SDH is commonly found in AHT and can increase head circumference, particularly in cases of repeated traumatic events from a very early age. SDH results from injury to bridging veins secondary to a combination of acceleration and abrupt deceleration, shearing, and rotational forces. The combination of SDH, retinal hemorrhage, and neurologic dysfunction is highly specific for AHT, also known as shaken-baby syndrome [16]. Signs of direct impact are often lacking [17]. Epidural hematomas in infants can cross cranial sutures, can occur without associated fracture, and are often due to venous injury [18].

At imaging, supratentorial SDH appears as crescentic collections frequently located along the convexity, the posterior falx, or the tentorium [19, 20]. Repeated hemorrhage can lead to formation of layers with variable signal intensity or attenuation related to blood products at different ages, with or without septations. Subdural hygromas can result from lacerations in the arachnoid through which CSF can migrate to the subdural space and accumulate rapidly. Therefore, hemorrhage from ruptured bridging veins and CSF from arachnoid lacerations can be mixed, resulting in hematoma-hygroma. For this reason, dating subdural collections is challenging.

Veins in the subarachnoid space can be seen abutting the brain parenchyma and compressed by the subdural collection (Fig. 1B). Thrombosis of bridging veins crossing the subdural space commonly occurs near the vertex and is best seen on coronal images (Fig. 1C) [21]. Images obtained with blood-sensitive sequences such as T2*-weighted gradient-recalled echo and susceptibility-weighted imaging may show a round area of decreased signal intensity along the course of a stretched bridging vein, representing clot ("lollipop" or "tadpole" sign) [22]. Other signs of abusive trauma include retinal hemorrhage (best seen on susceptibility-weighted images) [23, 24], cerebral contusions and lacerations, abnormal diastasis of the sutures, diffuse axonal injuries, and multiple fractures.

Glutaric aciduria type 1—Glutaric aciduria type 1 is a rare autosomal recessive neurometabolic disorder caused by a deficiency in glutaryl–coenzyme A dehydrogenase, which results in accumulation of glutaric acids with progressive hypotonia and neurologic deterioration [25]. Macrocephaly is a key finding and is usually present at birth or develops soon thereafter. This condition can also feature megalencephaly.

The most classic imaging sign, present in more than 90% of cases, is the finding of wide sylvian fissures with open opercula and enlarged CSF spaces anterior to the temporal lobe in addition to white matter edema. Metabolic crises can result in abnormal symmetric T2-hyperintensity of the basal ganglia, particularly the globi pallidi. The prevalence of spontaneous SDH has been estimated to be approximately 20–30% in patients with glutaric aciduria type 1 and can lead to a diagnostic pitfall, prompting suspicion of AHT. Although it is important to include AHT in the differential diagnosis of macrocephaly in children with SDH, the aforementioned classic imaging features should suggest glutaric aciduria type 1 as the cause [26] (Fig. 1D).

Enlarged Ventricles (Hydrocephalus)

Hydrocephalus is a disorder of CSF function and flow dynamics characterized by ventricular enlargement that presents with macrocephaly when onset is before 2 years of age. In most cases it is obstructive and can be classified as intraventricular (obstructive) or extraventricular (communicating). Intraventricular hydrocephalus is characterized by impaired flow of CSF through the foramen of Monro, Luschka, or Magendie or through the sylvian aqueduct. This is often secondary to mass lesions and is also commonly seen in the acute phase of intraventricular hemorrhage in premature infants. Extraventricular hydrocephalus results from impaired reabsorption of CSF at the level of the arachnoid granulations caused by either chronic accumulation of blood products or inflammatory scarring, that is, posthemorrhagic hydrocephalus or meningitis, respectively. Different mechanisms can often coexist. Overproduction hydrocephalus is rare but may be present in children with choroid plexus tumors.

Common radiologic features of hydrocephalus include downward bowing of the floor of the third ventricle with enlargement of the anterior and posterior recesses, best seen on sagittal images; dilatation of temporal horns; effacement of cerebral sulci; periventricular interstitial edema; stretching and thinning of the corpus callosum; and occasionally ventricular diverticula or pseudodiverticula [27, 28]. Children with hydrocephalus resulting in macrocephaly may also present with frontal bossing, thin skull with gyral markings ("copper beaten skull"), suture diastasis, and prominent diploic veins.

Congenital Hydrocephalus

Aqueductal stenosis—Aqueductal stenosis is the most common cause of congenital hydrocephalus, comprising 20% of cases, and is typically associated with macrocephaly [29]. Familial forms of hydrocephalus, including X-linked aqueductal stenosis caused by mutations in the *L1CAM* gene, have been de-

scribed [30]. Focal stenosis usually occurs at the level of the superior colliculi or the intercollicular sulcus (Fig. 2A). In some cases the aqueduct can be normal in width, and hydrocephalus is caused by a thin membrane of tissue in the distal aqueduct called the aqueductal web. The stenosis can also be extrinsic, as from compression by an arachnoid or choroid plexus cyst (Fig. 2B). An association exists between aqueductal stenosis and rhombencephalosynapsis, a rare malformation characterized by lack of separation of the cerebellar hemispheres in conjunction with variable vermian hypoplasia or aplasia [31]. Aqueductal stenosis can be treated by endoscopic third ventriculostomy, and radiologic studies are essential for preoperative planning and follow-up [32].

At imaging, supratentorial ventricular dilatation with inferior bulging of the third ventricular floor and a normal fourth ventricle can be appreciated with MRI as early as during the fetal period. High-resolution cisternographic images are useful in the postnatal period for determining the exact site of narrowing or of the web. Proximal stenosis usually causes more severe hydrocephalus, and more distal stenosis leads to a milder degree of ventricular dilatation. Funneling of the superior portion of the aqueduct may be present with formation of multiple anastomotic canaliculi (forking). There also can be associated fusion of the quadrigeminal bodies and third nerve nuclei [33].

Aqueductal stenosis may be a feature of complex brain malformations, including congenital muscular dystrophy (also known as dystroglycanopathy). The most severe form, Walker-Warburg syndrome, is characterized by cobblestone cortical malformation, supratentorial hydrocephalus, dysmorphic Z-shaped brainstem, and cerebellar dysplasia with cysts [34, 35] (Figs. 2C and 2D).

Chiari malformation type 2—Chiari malformation type 2 is the most common syndromic cause of hydrocephalus. It consists of a complex spectrum of encephalic and skull base anomalies, almost invariably associated with a non–skin-covered myelomeningocele [36]. The key cranial features of Chiari malformation type 2 are thought to result from a small posterior fossa caused by CSF leakage through the myelomeningocele. Supratentorial hydrocephalus, when not present at birth, usually develops after closure of the myelomeningocele, which generally occurs either prenatally or within 48 hours of birth. In addition to cerebellar tonsillar herniation, the foramina of Luschka and Magendie lie below the foramen magnum, directing most of the intracranial CSF outflow to the spinal canal [37, 38].

At imaging, almost all patients have different degrees of myelomeningocele. Once the defect is repaired, hydrocephalus and syringohydromyelia may develop. The classic cranial abnormality is a small posterior fossa with a flattened floor and crowding of cerebellar structures (Fig. 3A). The dorsal insertion of the cerebellar tentorium is low-lying, and the straight sinus has a vertical course. The fourth ventricle is usually slitlike. Cerebellar development ranges from near normality to severe hypoplasia. Cerebellar tonsillar herniation through the foramen magnum, with variable extension into the spinal canal, may be accompanied by herniation of the choroid plexus of the fourth ventricle. The cerebellum may herniate cranially through the tentorium (towering) and wrap around the brainstem. The pons is flattened. Tectal beaking may be present owing to fusion of the colliculi and lateral pressure from the temporal lobes. This can lead to morphologic anomalies of the sylvian aqueduct, which contribute to the supratentorial hydrocephalus. A cervicomedullary kink can also be present.

Hydrocephalus in Chiari malformation type 2 is common and features colpocephaly, a disproportionate enlargement of the atria and occipital horns. Given the very early onset of the malformation, the head is large and can look like a "copper beaten skull," which consists of impressions on the inner table of the calvaria due the pressure of cerebral gyri on the soft calvarial bones. Anomalies of the corpus callosum may be present. Gyral interdigitations between the two hemispheres may also be present, as may callosal dysgenesis. The caudate heads and interthalamic adhesions can be enlarged. Gray matter heterotopia can be caused by stretching of the cerebrum, which results in impaired migration of neuronal precursors from the ventricular zone to the cortical plate through the radial glial cells. Finally, although less common, hydrocephalus may also occur in Chiari malformations types 1 and 3.

Dandy-Walker malformation—Dandy-Walker malformation is characterized by a large posterior fossa with cystlike dilatation of the fourth ventricle and various degrees of cerebellar vermis hypoplasia (Fig. 3B). Macrocephaly is the most common manifestation, and in approximately 80% of cases, the diagnosis is made by the first year of life [39].

At imaging, the torcular herophili and the tentorium are elevated and lie above the lambdoid suture (torcular-lambdoid inversion). The cerebellar vermis is superiorly rotated and has different degrees of hypoplasia, up to complete agenesis. The enlarged fourth ventricle may exert a mass effect on the cerebellar hemispheres. Other CNS abnormalities may be present, such as heterotopia, polymicrogyria, schizencephaly, and callosal dysgenesis [40].

The most common differential diagnoses include arachnoid cyst, mega cisterna magna, and Blake pouch cyst. Large posterior fossa arachnoid cysts are separate from the fourth ventricle with a normally formed vermis. Large arachnoid cysts may cause scalloping of the calvaria and supratentorial hydrocephalus if compressing the fourth ventricle. Cisternographic sequences can help clarify the boundaries of each anatomic structure. Mega cisterna magna is not a mass lesion and does not compress nearby structures, nor does it impair CSF flow; hence, it does not cause hydrocephalus. The brainstem and cerebellum are normal [41]. Blake pouch cyst is an inferior outpouching of the fourth ventricle due to unruptured foramen of Magendie. The ventricle may be normal or compressed, resulting in hydrocephalus, and its choroid plexus can protrude into the cyst. Depending on cyst size, there may be cerebellar compression with upward displacement of the vermis, but cerebellar structure should be normal without vermian hypoplasia.

There is some confusion in the literature regarding the classification of cystic anomalies of the posterior fossa. In particular, the term "Dandy-Walker variant" is used to describe abnormalities with an unrelated etiologic factor, such as arachnoid cysts and inferior vermian hypoplasia. When one is faced with a cystic anomaly of the posterior fossa, detailed description of morphologic characteristics should be favored, and labels such as "Dandy-Walker variant" should be avoided.

Acquired Hydrocephalus

Posthemorrhagic hydrocephalus—Hydrocephalus is a frequent sequela of intraventricular hemorrhage in preterm infants with germinal matrix–intraventricular hemorrhage spectrum [42]. Approximately 20% of infants born before 34 weeks' gestation have germinal matrix hemorrhage, which can be complicated by intraventricular extension. These patients can have acute hydrocephalus and periventricular venous infarctions secondary to subependymal venous compres-

sion. Later development of posthemorrhagic obstructive hydrocephalus from arachnoiditis of the choroid villi induced by evolving blood products complicates 35% of cases. As many as 15% of these children eventually need ventriculoperitoneal shunting [43] (Figs. 4A and 4B).

Head ultrasound is the best imaging modality for monitoring hydrocephalus in the acute and subacute phases. Imaging shows hydrocephalus most commonly affecting the supratentorial ventricles, which can be severely dilated with marked parenchymal compression. Entrapment of the fourth ventricle resulting in marked dilatation is commonly seen in preterm infants and should not be confused with Dandy-Walker malformation. Areas of gliosis with cystic encephalomalacia in the periventricular white matter are common sequelae of periventricular hemorrhagic venous infarctions and can exhibit blooming artifact on susceptibility-weighted images owing to hemosiderin deposition.

Postinfectious hydrocephalus—Postinfectious hydrocephalus in infants is the result of purulent or granulomatous arachnoiditis or aqueductal stenosis. A component of compensatory (ex vacuo) ventriculomegaly can occur after parenchymal volume loss or destruction. The presence of inflammatory exudate leads to arachnoiditis, which can result in chronic hydrocephalus and macrocephaly. Toxoplasmosis is the most common cause of postinfectious hydrocephalus in infants, particularly in developing countries. Fungal and granulomatous meningitides are more likely to cause clinically significant hydrocephalus than are bacterial and viral infections [44].

Hydrocephalus Due to Tumors

Pineal region tumors—Neoplasms occurring in the pineal region can cause aqueductal obstruction and thus present with supratentorial hydrocephalus. Germinomas are the most common tumors of the pineal region. They are heterogeneous, avidly enhancing hypercellular lesions that exhibit restricted diffusion, high attenuation at CT, and low T2 signal intensity to adjacent brain. Mild restricted diffusion reflects high cellularity. Hemorrhage is common. The tumor appears to engulf the pineal gland and often invades the nearby brain parenchyma [45].

Teratomas constitute 26–50% of fetal intracranial neoplasms, and they can cause congenital hydrocephalus [46]. They exhibit heterogeneous attenuation and signal intensity with the characteristic presence of fat, calcifications, and cystic elements [47] (Fig. 5).

Pineoblastomas are usually seen in younger children as large, heterogeneous hypercellular masses with necrosis, hemorrhage, and peripheral calcifications. Diffusion is restricted to a larger degree than in germinomas, and ADC values are markedly low [48].

Posterior fossa tumors—Medulloblastoma is the most common infratentorial malignant brain tumor of childhood. The tumor is a hypercellular, usually midline mass protruding into and effacing the fourth ventricle with resulting supratentorial hydrocephalus (Figs. 6A and 6B). Brainstem and cerebellar invasion is common, as is leptomeningeal seeding in the spinal canal at presentation [49]. Medulloblastoma usually exhibits diffusion restriction due to its high cellularity and is currently categorized in four molecular subgroups [50]. Enhancement is variable [51].

Infratentorial pilocytic astrocytomas are usually centered in the cerebellar hemispheres. They are T2-hyperintense masses with variable nodular enhancement, high ADC values reflecting low cellularity, and often (but not always) an associated cystic component.

When a young child presents with a hypercellular infiltrative mass in the posterior fossa containing blood products and calcifications, atypical teratoid rhabdoid tumor should be considered, although definitive diagnosis can be achieved only with immunohistochemical analysis [52].

Ependymoma usually arises within the fourth ventricle and extends through the foramina of Luschka and Magendie with cisternal involvement. It is extremely heterogeneous and can have varied signal intensity and attenuation characteristics, usually with avid enhancement. Calcifications and hemorrhage are seen more often than in medulloblastoma (Figs. 6C and 6D).

Increased CSF production—Choroid plexus tumors can cause hydrocephalus secondary to excessive CSF production, although an obstructive component may be superimposed by hemorrhage or leptomeningeal dissemination. Choroid plexus papillomas are classified as World Health Organization (WHO) grade I lesions (II if atypical) and are far more common than choroid plexus carcinomas (WHO grade IV) [53]. Choroid plexus carcinomas are large invasive tumors with a tendency to recur [54, 55].

Imaging shows that choroid plexus tumors are solid, avidly enhancing intraventricular masses more often presenting in the atria of the lateral ventricles. Speckled calcifications are present in 25% of cases. Large tumors with markedly heterogeneous signal intensity, central necrosis, and hemorrhagic elements should raise suspicion of choroid plexus carcinoma. In such tumors, cerebral invasion is characterized by abnormal signal intensity of the adjacent brain parenchyma (Fig. 7).

Vascular anomalies—Vein of Galen aneurysmal malformation (VGAM) can cause obstructive hydrocephalus secondary to mass effect on the third ventricle and sylvian aqueduct and communicating hydrocephalus due to chronically increased venous pressure leading to impaired CSF reabsorption. Classic features seen at fetal or neonatal MRI include persistence of the median prosencephalic vein, which appears as a large flow void on T2-weighted images, usually with dilated and tortuous choroidal and anterior cerebral artery feeders. In VGAM, ischemia due to venous congestion results in white matter injury in the developing brain, which may manifest as volume loss or white matter calcifications. Rapid progression of subependymal atrophy with ventricular dilatation may occur [56] and is known as "melting brain."

Megalencephaly

Megalencephaly is a condition in which the size or weight of the brain is greater than 2 SD above the age-related mean. It is classified as developmental or metabolic, both of which have underlying genetic causes. Developmental megalencephaly is secondary to signal pathway alterations affecting cellular replication or apoptosis that result in an increased number or size of neurons or both. In contrast, metabolic megalencephaly is secondary to metabolic errors and has a variable age at onset after abnormal metabolites have accumulated in the neural cells. Regardless of the cause, megalencephaly syndromes are characterized by increased volume of brain parenchyma in the absence of increased intracranial pressure [1, 57].

Developmental megalencephaly—Most of these disorders involve the mechanistic target of rapamycin (mTOR), the Ras/mitogen-activated protein kinase (MAPK) pathway, and other transcriptional regulators. Hemimegalencephaly, also known as dysplastic megalencephaly, is secondary to alterations of the mTOR pathway and can be associated with phakomatoses such as tuberous sclerosis complex and neurofibromatosis type 1 or with syndromes associated with vascular anomalies, such as Proteus syndrome; congenital lipomatous overgrowth, vascular

malformations, epidermal nevi, and skeletal and spinal anomalies (CLOVES) syndrome; and epidermal nevus syndrome. It is characterized by marked congenital macrocephaly with dysplastic and asymmetric overgrowth of the entirety or part of one cerebral hemisphere. The affected hemisphere is dysplastic and may have the appearance of lissencephaly or polymicrogyria. The contralateral hemisphere is usually normal in appearance, although bilateral asymmetric involvement has been reported [58]. Most often the affected lateral ventricle has a characteristic shape of the frontal horn, which appears straight, narrow, and pointing superiorly [59] (Fig. 8).

Other rare syndromes include megalencephaly–capillary malformation–polymicrogyria syndrome (MCAP) and megalencephaly-polymicrogyria-polydactyly-hydrocephalus (MPPH), also secondary to alterations of the mTOR pathway [60]. Cerebral gigantism, or Sotos syndrome, is characterized by macrocephaly, intellectual disability (mental retardation), callosal dysgenesis, and ventriculomegaly with colpocephaly.

Metabolic megalencephaly—Alexander disease is an autosomal dominant disease caused by mutations that result in accumulation of glial fibrillary acidic protein (GFAP) within astrocytes. This results in abnormal myelination, possibly secondary to disrupted astrocyte-oligodendrocyte interaction [61]. The disease most commonly presents in infancy with early onset of macrocephaly and rapid neurologic deterioration leading to early death. Neonatal and juvenile variants, respectively more and less severe, have also been described [62]. Alexander disease is one of a few neurometabolic disorders with specific MRI features (Fig. 9A). To establish the diagnosis, four of the five following criteria must be present [63]: extensive cerebral white matter abnormalities most prominent in the frontal lobes; a periventricular T1-hyperintense T2-hypointense peripheral rim; heterogeneous abnormal signal intensity of the basal ganglia and thalami; medulla and midbrain signal-intensity abnormalities; and contrast enhancement of one or more of ventricular lining, periventricular rim, frontal white matter, optic chiasm, fornix, basal ganglia, thalamus, dentate nucleus, or brainstem. Garlandlike enhancement anterior to the frontal horns is characteristic [64].

Canavan disease is an autosomal recessive disorder of glial degeneration due to mutations that cause accumulation of *N*-acetylaspartate (NAA) in oligodendrocytes that results in myelin vacuolization and glial swelling. The disease presents with macrocephaly, lack of head control, and developmental delay that progresses with hypotonia and eventually ends in spasticity. Death usually occurs in the second year of life, although some patients survive longer than 10 years [65]. At imaging, children present with symmetric, extensive areas of T1-hypointensity and T2-hyperintensity involving subcortical white matter fibers early in the course of the disease (Fig. 9B). The pathognomonic finding is a very high peak of NAA at MR spectroscopy (Fig. 9C). The spectrum may resemble that of a normally developed adult but is the opposite of the one of a healthy child of that age [66]. In advanced cases, marked cerebral atrophy develops.

Mucopolysaccharidosis and other lysosomal storage disorders, such as Hurler, Hunter, and Tay-Sachs diseases, cause macrocephaly secondary to hydrocephalus that develops owing to accumulation of metabolites in the perivascular spaces and meninges with secondary impairment of CSF reabsorption.

Megalencephalic leukoencephalopathy with subcortical cysts is a rare autosomal recessive disorder usually presenting at approximately 2 years of age with progressive ataxia and dysarthria. MRI is characterized by diffuse swelling and T2 hyperintensity of the white matter with characteristic subcortical cysts [67] (Fig. 9D).

Osseous Abnormalities

Achondroplasia presents with marked macrocephaly at birth that worsens in the first year of life. The membranous cranial vault is disproportionately large compared with the hypoplastic skull base with associated frontal bossing and depression of the nasion. Children with achondroplasia may have hydrocephalus, which may contribute to the head enlargement (Fig. 10A). Mechanisms include intracranial venous hypertension due to jugular foraminal hypoplasia and CSF flow disturbance due to a small foramen magnum [68].

Hematologic disorders such as thalassemia major may cause macrocephaly secondary to extramedullary hematopoiesis with extensive calvarial thickening and a "hairy" appearance of the vault on radiographs (Fig. 10B).

Conclusion

Macrocephaly can be the presenting clinical finding in a range of neurologic conditions that range from benign enlargement of subarachnoid spaces to tumors and metabolic disorders resulting from abnormal prenatal or postnatal increases in the volume of one of the intracranial compartments while the cranial sutures are open. By using a systematic approach to neuroimaging acquisition and interpretation, radiologists help establish correct diagnoses and guide management.

References

1. Winden KD, Yuskaitis CJ, Poduri A. Megalencephaly and macrocephaly. *Semin Neurol* 2015; 35:277–287
2. Mokri B. The Monro-Kellie hypothesis: applications in CSF volume depletion. *Neurology* 2001; 56:1746–1748
3. Weinzweig J, Kirschner RE, Farley A, et al. Metopic synostosis: defining the temporal sequence of normal suture fusion and differentiating it from synostosis on the basis of computed tomography images. *Plast Reconstr Surg* 2003; 112:1211–1218
4. Kiesler J, Ricer R. The abnormal fontanel. *Am Fam Physician* 2003; 67:2547–2552
5. Williams CA, Dagli A, Battaglia A. Genetic disorders associated with macrocephaly. *Am J Med Genet A* 2008; 146:2023–2037
6. Davenport MS, Wang CL, Bashir MR, Neville AM, Paulson EK. Rate of contrast material extravasations and allergic-like reactions: effect of extrinsic warming of low-osmolality iodinated CT contrast material to 37 degrees C. *Radiology* 2012; 262:475–484
7. Smith R, Leonidas JC, Maytal J. The value of head ultrasound in infants with macrocephaly. *Pediatr Radiol* 1998; 28:143–146
8. Stoquart-El Sankari S, Lehmann P, Gondry-Jouet C, et al. Phase-contrast MR imaging support for the diagnosis of aqueductal stenosis. *AJNR* 2009; 30:209–214
9. Hamza M, Bodensteiner JB, Noorani PA, Barnes PD. Benign extracerebral fluid collections: a cause of macrocrania in infancy. *Pediatr Neurol* 1987; 3:218–221
10. Medina LS, Frawley K, Zurakowski D, Buttros D, DeGrauw AJ, Crone KR. Children with macrocrania: clinical and imaging predictors of disorders requiring surgery. *AJNR* 2001; 22:564–570
11. Maytal J, Alvarez LA, Elkin CM, Shinnar S. External hydrocephalus: radiologic spectrum and differentiation from cerebral atrophy. *AJR* 1987; 148:1223–1230
12. Paciorkowski AR, Greenstein RM. When is enlargement of the subarachnoid spaces not benign? A genetic perspective. *Pediatr Neurol* 2007; 37:1–7
13. Tucker J, Choudhary AK, Piatt J. Macrocephaly in infancy: benign enlargement of the subarachnoid spaces and subdural collections. *J Neurosurg Pediatr* 2016; 18:16–20
14. McNeely PD, Atkinson JD, Saigal G, O'Gorman AM, Farmer JP. Subdural hematomas in infants

with benign enlargement of the subarachnoid spaces are not pathognomonic for child abuse. *AJNR* 2006; 27:1725–1728

15. Fernando S, Obaldo RE, Walsh IR, Lowe LH. Neuroimaging of nonaccidental head trauma: pitfalls and controversies. *Pediatr Radiol* 2008; 38:827–838
16. Duhaime AC, Christian CW, Rorke LB, Zimmerman RA. Nonaccidental head injury in infants: the "shaken-baby syndrome". *N Engl J Med* 1998; 338:1822–1829
17. Miller D, Barnes P, Miller M. The significance of macrocephaly or enlarging head circumference in infants with the triad: further evidence of mimics of shaken baby syndrome. *Am J Forensic Med Pathol* 2015; 36:111–120
18. Huisman TA, Tschirch FT. Epidural hematoma in children: do cranial sutures act as a barrier? *J Neuroradiol* 2009; 36:93–97
19. Pinto PS, Meoded A, Poretti A, Tekes A, Huisman TA. The unique features of traumatic brain injury in children. review of the characteristics of the pediatric skull and brain, mechanisms of trauma, patterns of injury, complications, and their imaging findings–part 2. *J Neuroimaging* 2012; 22:e18–e41
20. Pierce MC, Bertocci GE, Berger R, Vogeley E. Injury biomechanics for aiding in the diagnosis of abusive head trauma. *Neurosurg Clin N Am* 2002; 13:155–168
21. Zuccoli G, Khan AS, Panigrahy A, Tamber MS. In vivo demonstration of traumatic rupture of the bridging veins in abusive head trauma. *Pediatr Neurol* 2017; 72:31–35
22. Choudhary AK, Bradford R, Dias MS, Thamburaj K, Boal DK. Venous injury in abusive head trauma. *Pediatr Radiol* 2015; 45:1803–1813
23. Zuccoli G, Panigrahy A, Haldipur A, et al. Susceptibility weighted imaging depicts retinal hemorrhages in abusive head trauma. *Neuroradiology* 2013; 55:889–893
24. Polan RM, Poretti A, Scheller JM, Huisman TA, Bosemani T. Retinal hemorrhages in nonaccidental trauma: look at susceptibility-weighted imaging on pediatric MRI. *Pediatr Neurol* 2015; 52:464–465
25. Hoffmann GF, Trefz FK, Barth PG, et al. Macrocephaly: an important indication for organic acid analysis. *J Inherit Metab Dis* 1991; 14:329–332
26. Vester ME, Bilo RA, Karst WA, Daams JG, Duijst WL, van Rijn RR. Subdural hematomas: glutaric aciduria type 1 or abusive head trauma? A systematic review. *Forensic Sci Med Pathol* 2015; 11:405–415
27. Manara R, Citton V, Traverso A, et al. Intraparenchymal ventricular diverticula in chronic obstructive hydrocephalus: prevalence, imaging features and evolution. *Acta Neurochir (Wien)* 2015; 157:1721–1730
28. Calloni SF, Soares BP, Huisman TA. Ventricular pseudodiverticula from intraparenchymal cerebrospinal fluid dissection secondary to high-grade obstructive hydrocephalus in children: magnetic resonance imaging findings. *Neuroradiol J* 2017; 30:425–428
29. Wright Z, Larrew TW, Eskandari R. Pediatric hydrocephalus: current state of diagnosis and treatment. *Pediatr Rev* 2016; 37:478–490
30. Shaheen R, Sebai MA, Patel N, et al. The genetic landscape of familial congenital hydrocephalus. *Ann Neurol* 2017; 81:890–897
31. Whitehead MT, Choudhri AF, Grimm J, Nelson MD. Rhombencephalosynapsis as a cause of aqueductal stenosis: an under-recognized association in hydrocephalic children. *Pediatr Radiol* 2014; 44:849–856
32. Maller VV, Gray RI. Noncommunicating Hydrocephalus. *Semin Ultrasound CT MR* 2016; 37:109–119
33. Barkovich AJ, Newton TH. MR of aqueductal stenosis: evidence of a broad spectrum of tectal distortion. *AJNR* 1989; 10:471–476
34. Barkovich AJ. Neuroimaging manifestations and classification of congenital muscular dystrophies. *AJNR* 1998; 19:1389–1396
35. Clement E, Mercuri E, Godfrey C, et al. Brain involvement in muscular dystrophies with defective dystroglycan glycosylation. *Ann Neurol* 2008; 64:573–582
36. Radbruch A, Weberling LD, Kieslich PJ, et al. Gadolinium retention in the dentate nucleus and globus pallidus is dependent on the class of contrast agent. *Radiology* 2015; 275:783–791
37. Rintoul NE, Sutton LN, Hubbard AM, et al. A new look at myelomeningoceles: functional level, vertebral level, shunting, and the implications for fetal intervention. *Pediatrics* 2002; 109:409–413
38. McLone DG, Naidich TP. Developmental morphology of the subarachnoid space, brain vasculature, and contiguous structures, and the cause of the Chiari II malformation. *AJNR* 1992; 13:463–482
39. Kollias SS, Ball WS Jr, Prenger EC. Cystic malformations of the posterior fossa: differential diagnosis clarified through embryologic analysis. *RadioGraphics* 1993; 13:1211–1231
40. Correa GG, Amaral LF, Vedolin LM. Neuroimaging of Dandy-Walker malformation: new concepts. *Top Magn Reson Imaging* 2011; 22:303–312
41. Shekdar K. Posterior fossa malformations. *Semin Ultrasound CT MR* 2011; 32:228–241
42. Kulkarni AV, Riva-Cambrin J, Butler J, et al. Outcomes of CSF shunting in children: comparison of Hydrocephalus Clinical Research Network cohort with historical controls: clinical article. *J Neurosurg Pediatr* 2013; 12:334–338
43. Kazan S, Gura A, Ucar T, Korkmaz E, Ongun H, Akyuz M. Hydrocephalus after intraventricular hemorrhage in preterm and low-birth weight infants: analysis of associated risk factors for ventriculoperitoneal shunting. *Surg Neurol* 2005; 64(suppl 2):S77–S81; discussion, S81
44. Hutson SL, Wheeler KM, McLone D, et al. Patterns of hydrocephalus caused by congenital *Toxoplasma gondii* infection associate with parasite genetics. *Clin Infect Dis* 2015; 61:1831–1834
45. Kilgore DP, Strother CM, Starshak RJ, Haughton VM. Pineal germinoma: MR imaging. *Radiology* 1986; 158:435–438
46. Sandow BA, Dory CE, Aguiar MA, Abuhamad AZ. Best cases from the AFIP: congenital intracranial teratoma. *RadioGraphics* 2004; 24:1165–1170
47. Storr U, Rupprecht T, Bornemann A, et al. Congenital intracerebral teratoma: a rare differential diagnosis in newborn hydrocephalus. *Pediatr Radiol* 1997; 27:262–264
48. Dumrongpisutikul N, Intrapiromkul J, Yousem DM. Distinguishing between germinomas and pineal cell tumors on MR imaging. *AJNR* 2012; 33:550–555
49. Koeller KK, Rushing EJ. From the archives of the AFIP: medulloblastoma: a comprehensive review with radiologic-pathologic correlation. *RadioGraphics* 2003; 23:1613–1637
50. Perreault S, Ramaswamy V, Achrol AS, et al. MRI surrogates for molecular subgroups of medulloblastoma. *AJNR* 2014; 35:1263–1269
51. Koeller KK, Sandberg GD. From the archives of the AFIP. Cerebral intraventricular neoplasms: radiologic-pathologic correlation. *RadioGraphics* 2002; 22:1473–1505
52. Brandão LA, Young Poussaint T. Posterior fossa tumors. *Neuroimaging Clin N Am* 2017; 27:1–37
53. Gupta N. Choroid plexus tumors in children. *Neurosurg Clin N Am* 2003; 14:621–631
54. Connor SE, Chandler C, Bodi I, Robinson S, Jarosz JM. Preoperative and early postoperative magnetic resonance imaging in two cases of childhood choroid plexus carcinoma. *Eur Radiol* 2002; 12:883–888
55. Chopra K, Iyer S, Matta SK, Gupta A, Malhotra V. Choroid plexus carcinoma. *Indian Pediatr* 1996; 33:420–422
56. Chow ML, Cooke DL, Fullerton HJ, et al. Radiological and clinical features of vein of Galen malformations. *J Neurointerv Surg* 2015; 7:443–448
57. Mirzaa GM, Poduri A. Megalencephaly and hemimegalencephaly: breakthroughs in molecular etiology. *Am J Med Genet C Semin Med Genet* 2014; 166C:156–172
58. Parrini E, Conti V, Dobyns WB, Guerrini R. Genetic basis of brain malformations. *Mol Syndromol* 2016; 7:220–233
59. Broumandi DD, Hayward UM, Benzian JM, Gonzalez I, Nelson MD. Best cases from the AFIP: hemimegalencephaly. *RadioGraphics* 2004; 24:843–848
60. Cesmebasi A, Loukas M, Hogan E, Kralovic S,

Tubbs RS, Cohen-Gadol AA. The Chiari malformations: a review with emphasis on anatomical traits. *Clin Anat* 2015; 28:184–194

61. Srivastava S, Naidu S. Alexander disease. In: Pagon RA, Adam MP, Ardinger HH, et al., eds. *GeneReviews*. Seattle, WA: University of Washington, 1993
62. Springer S, Erlewein R, Naegele T, et al. Alexander disease: classification revisited and isolation of a neonatal form. *Neuropediatrics* 2000; 31:86–92
63. van der Knaap MS, Naidu S, Breiter SN, et al. Alexander disease: diagnosis with MR imaging. *AJNR* 2001; 22:541–552
64. van der Knaap MS, Ramesh V, Schiffmann R, et al. Alexander disease: ventricular garlands and abnormalities of the medulla and spinal cord. *Neurology* 2006; 66:494–498
65. Rodriguez D. Leukodystrophies with astrocytic dysfunction. *Handb Clin Neurol* 2013; 113:1619–1628
66. Michel SJ, Given CA 2nd. Case 99: Canavan disease. *Radiology* 2006; 241:310–314
67. van der Knaap MS, Boor I, Estévez R. Megalencephalic leukoencephalopathy with subcortical cysts: chronic white matter oedema due to a defect in brain ion and water homoeostasis. *Lancet Neurol* 2012; 11:973–985
68. Gordon N. The neurological complications of achondroplasia. *Brain Dev* 2000; 22:3–7

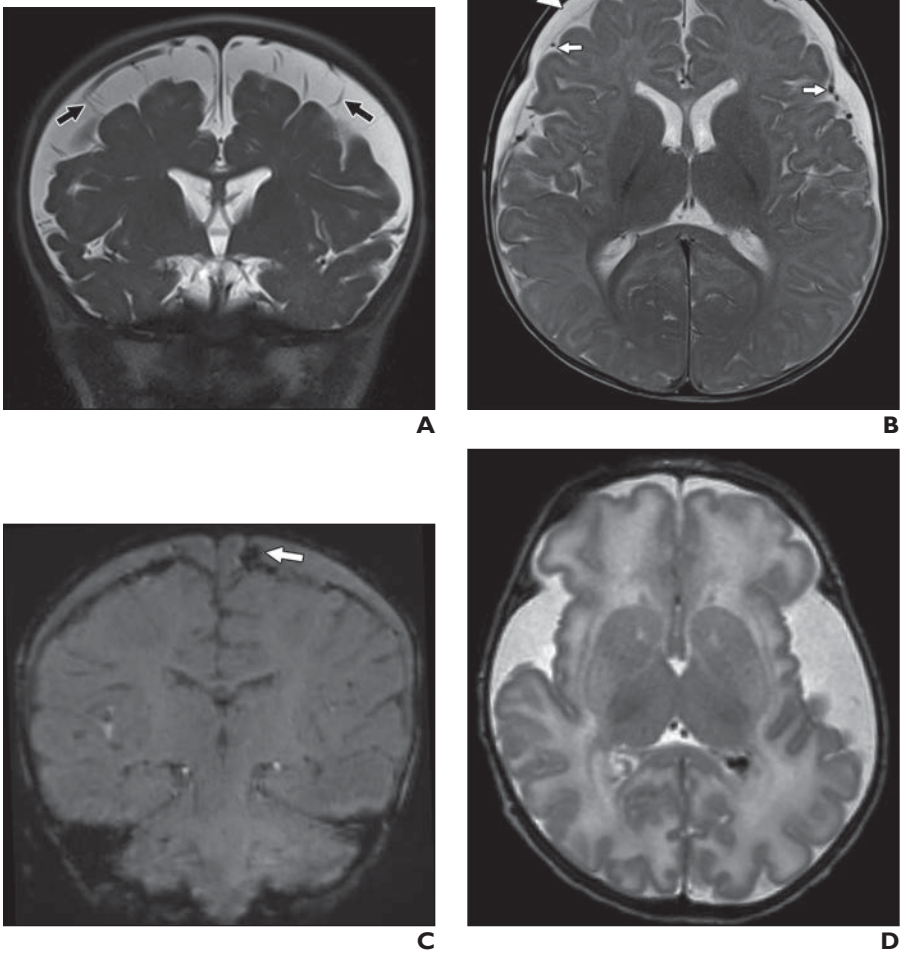

Fig. 1—Different causes of enlargement of extraaxial spaces manifesting as macrocephaly.
A, 11-month-old boy with macrocephaly and normal development. Example of benign enlargement of subarachnoid spaces. Coronal T2-weighted MR image shows enlarged subarachnoid spaces with crossing bridging veins (*arrows*) without associated mass effect.
B, 6-month-old girl admitted with altered mental status due to abusive head trauma. Axial T2-weighted MR image shows bilateral CSF-like subdural collections (*large arrows*) compressing subarachnoid veins (*small arrows*) on parenchymal surface.
C, 6-month-old girl admitted with altered mental status due to abusive head trauma (same patient as in **B**). Coronal susceptibility-weighted MR image shows bilateral subdural collections and foci of blooming artifact (*arrow*) on surface of brain, representing bridging veins thrombosis (lollipop sign).
D, 2-week-old girl with acute encephalopathy due to glutaric aciduria type 1. Axial T2-weighted MR image shows marked widening of sylvian fissures and bilateral hyperintensity in dorsal putamina.

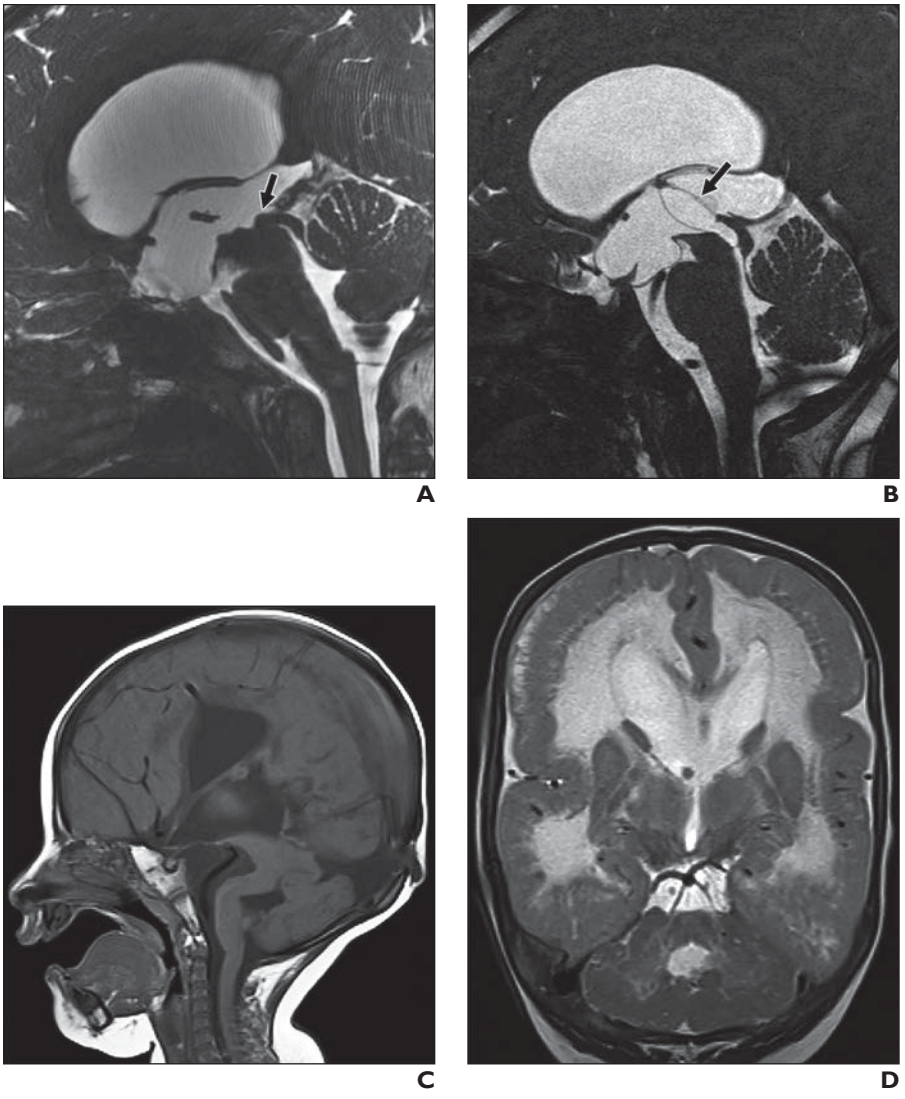

Fig. 2—Intrinsic and extrinsic aqueductal stenosis.
A, 9-month-old boy with congenital aqueductal stenosis. Sagittal cisternographic image shows high-grade stenosis (*arrow*) of sylvian aqueduct at level of superior colliculi resulting supratentorial hydrocephalus.
B, 3-year-old boy with choroid plexus cyst. Sagittal cisternographic image shows aqueductal obstruction by third ventricular choroid plexus cyst (*arrow*). (Courtesy of Martin KW, UCSF Benioff Children's Hospital, Oakland,Oakland, CA)
C, 4-month-old boy with macrocephaly due to Walker-Warburg syndrome. Sagittal T1-weighted MR image shows markedly dysplastic brainstem and shunted hydrocephalus.
D, 4-month-old boy with macrocephaly due to Walker-Warburg syndrome (same patient as in **C**). Coronal T2-weighted MR image shows cobblestone cortical malformation, diffusely abnormal white matter signal intensity, and extensive cerebellar dysplasia with microcysts.

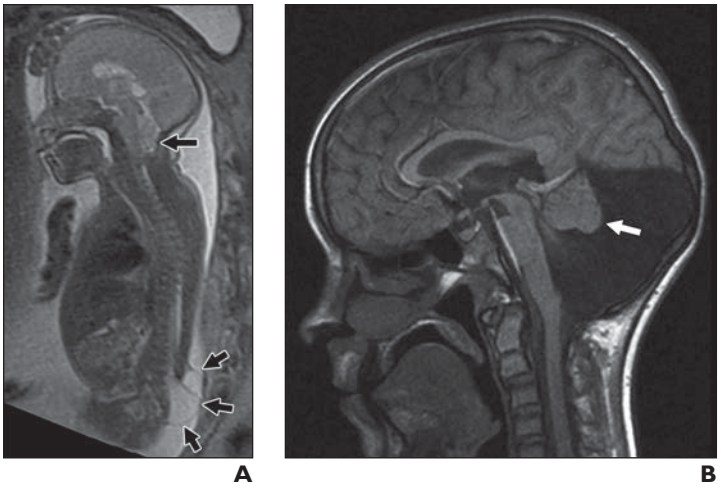

Fig. 3—Congenital hydrocephalus secondary to abnormalities of posterior fossa.
A, 2nd-trimester female fetus with Chiari malformation type 2. Sagittal T2-weighted MR image shows downward herniation of cerebellum (*large arrow*) and effacement of fourth ventricle associated with lumbosacral myelomeningocele (*small arrows*).
B, 3-year-old boy with macrocephaly due to Dandy-Walker malformation. Sagittal T1-weighted MR image shows cystic dilatation of fourth ventricle in enlarged posterior fossa with vermian hypoplasia (*arrow*).

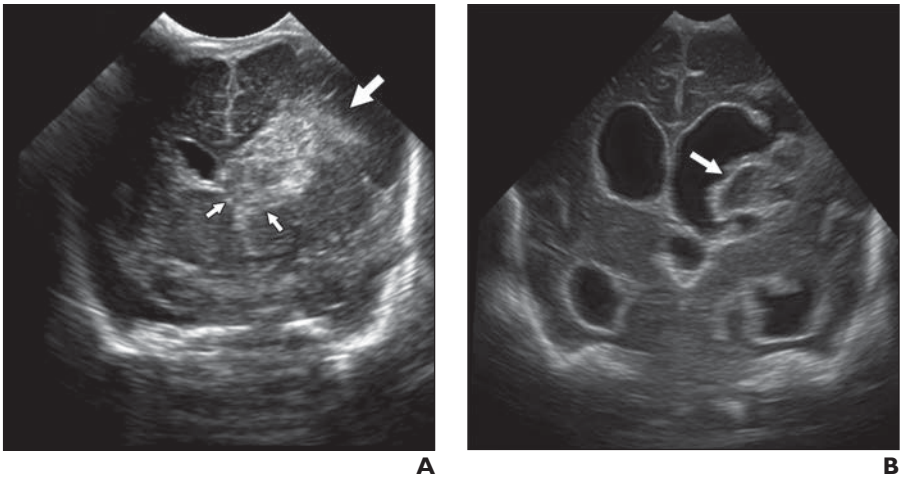

Fig. 4—Male infant born at 27 weeks' gestation. Example of posthemorrhagic hydrocephalus.
A, Coronal head ultrasound image through anterior fontanelle obtained at 4 days of life shows large left intraventricular hemorrhage (*small arrows*) with periventricular venous infarction (*large arrow*).
B, Coronal head ultrasound through anterior fontanelle obtained at 26 days of life shows evolving intraventricular hemorrhage (*arrow*) and infarction with interval development of hydrocephalus. Reactive hyperechogenic ependymal lining is evident.

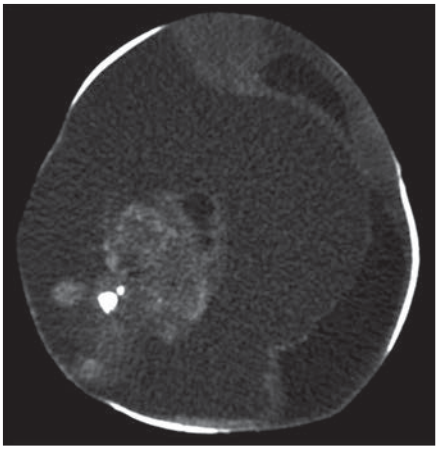

Fig. 5—2-day-old boy with congenital intracranial teratoma. Axial CT image shows heterogeneous solid and cystic attenuation with mixed calcified and fat components. Diastasis of sutures is evident. (Courtesy of Dupree B, Overton-Brooks VA Medical Center,Shreveport, LA)

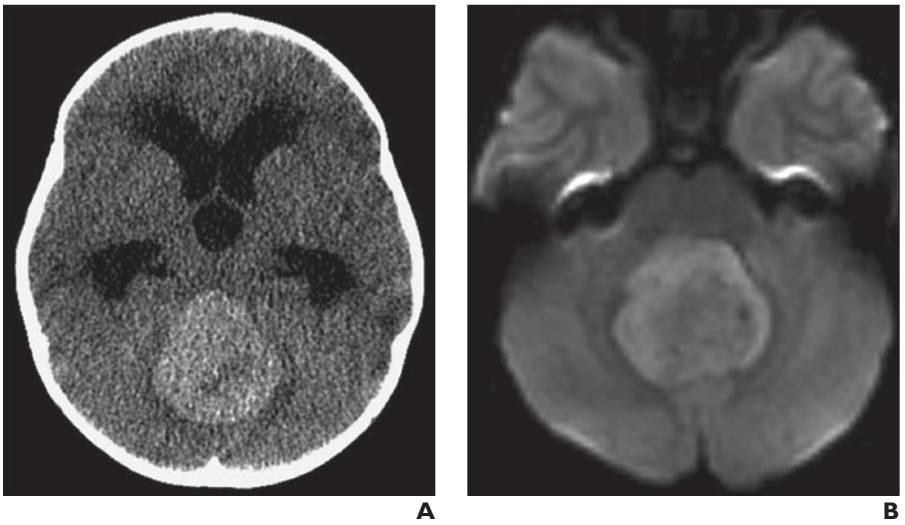

Fig. 6—Posterior fossa tumors presenting with macrocephaly.
A, 5-year-old boy with medulloblastoma. Axial unenhanced CT image shows high-attenuation midline lesion with effacement of fourth ventricle and associated moderate supratentorial hydrocephalus with periventricular interstitial edema. No clinically significant peritumoral vasogenic edema is present.
B, 5-year-old boy with medulloblastoma (same patient as in **A**). Axial trace DW image shows predominantly hyperintense mass. Apparent diffusion coefficient map (not shown) showed low signal intensity, confirming restricted diffusion. Both high attenuation on CT images and restricted diffusion on MR images indicate high cellularity.
(Fig. 6 continues on next page)

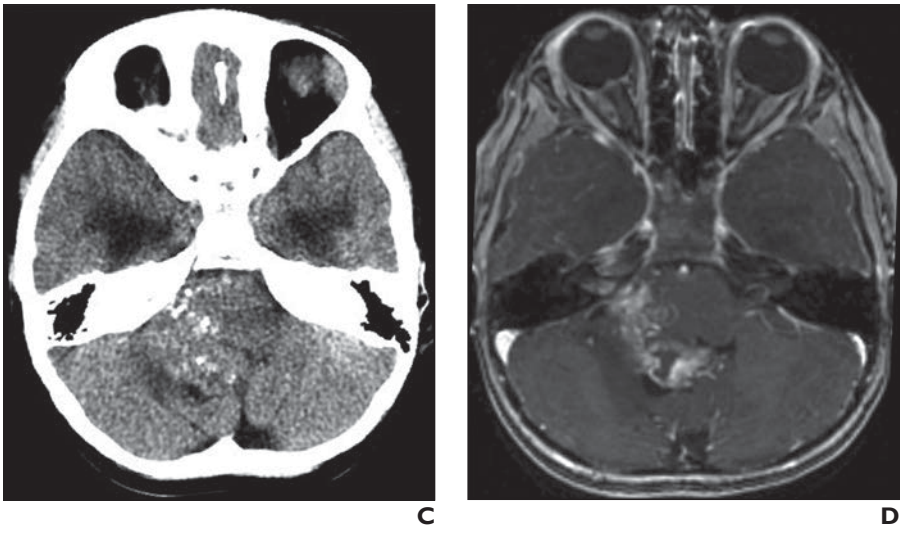

Fig. 6 (continued)—Posterior fossa tumors presenting with macrocephaly.
C, 4-year-old girl with ependymoma. Axial CT image shows heterogeneous mass containing stippled calcifications occupying fourth ventricle and extending through right foramen of Luschka.
D, 4-year-old girl with ependymoma (same patient as in **C**). Axial contrast-enhanced T1-weighted MR image shows heterogeneous enhancement of mass extending to right cerebellopontine angle and internal auditory canal.

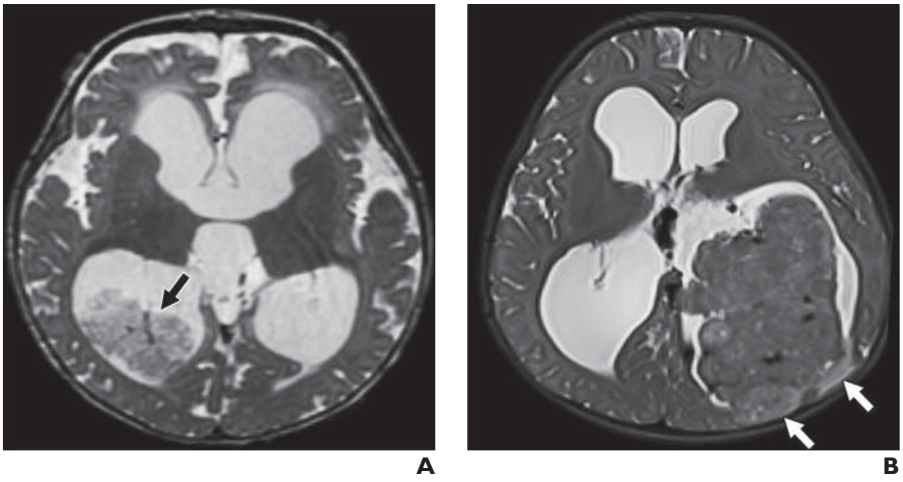

Fig. 7—Choroid plexus tumors resulting in hydrocephalus from overproduction of CSF.
A, 11-month-old girl with choroid plexus papilloma. Coronal T2-weighted MR image shows well-circumscribed lesion (*arrow*) in atrium of left lateral ventricle.
B, 2-year-old boy with choroid plexus carcinoma. Axial T2-weighted MR image shows large heterogeneous intraventricular mass and marked hydrocephalus. Invasion of posterior periventricular parenchyma (*arrows*) is evident.

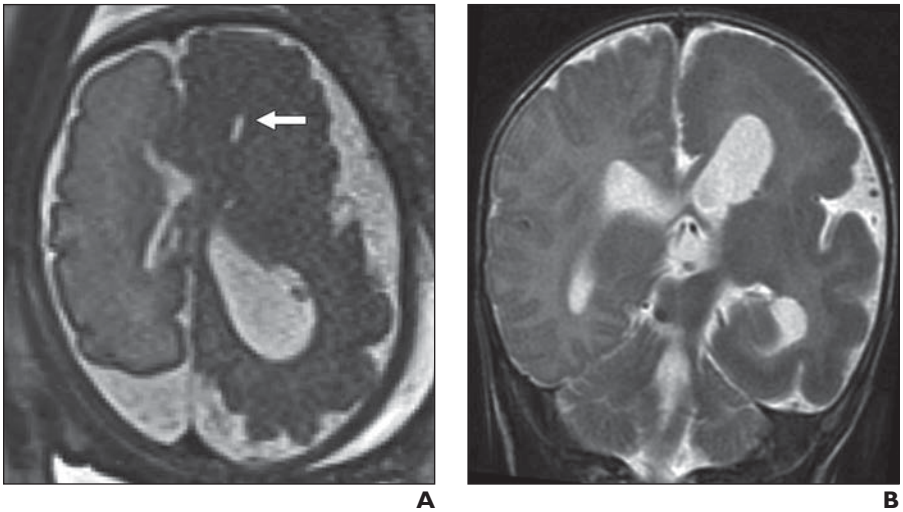

Fig. 8—Developmental megalencephaly.
A, Third-trimester male fetus with hemimegalencephaly. Fetal MR image shows enlargement of entire left hemisphere and abnormal gyration of cortex compared with contralateral, normal-appearing hemisphere. Asymmetric ventricular dilatation is present, except in frontal horn (*arrow*), which is characteristically straight and directed anteriorly.
B, 6-month-old boy with hemimegalencephaly. Coronal T2-weighted MR image shows enlarged left hemisphere with diffusely abnormal cortex and white matter. Enlarged left ventricle has characteristic shape with pointed anterior horn.

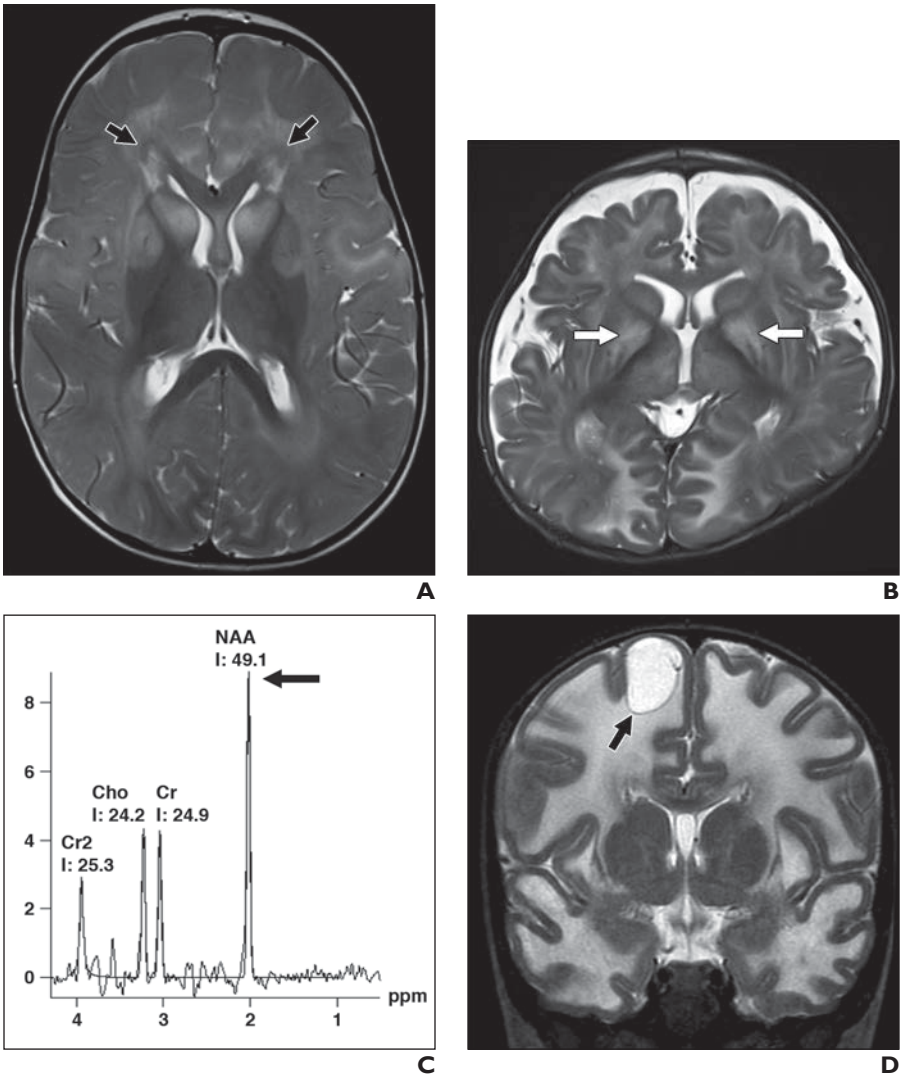

Fig. 9—Causes of metabolic megalencephaly.
A, 2-year-old boy with macrocephaly who has not reached developmental milestones owing to Alexander disease. Axial T2-weighted MR image shows frontal white matter edema with halo of T2-hypointensity anterior to frontal horns (*arrows*) and symmetric swelling and abnormal signal intensity of caudate heads and ventral putamina.
B, 4-month-old girl with macrocephaly, hypotonia, and developmental delay due to Canavan disease. T2-weighted MR image shows diffuse white matter signal-intensity abnormality, including subcortical U fibers, and basal ganglia involvement, particularly in globi pallidi.
C, 4-month-old girl with macrocephaly, hypotonia, and developmental delay due to Canavan disease (same patient as in **B**). MR spectroscopic readout shows *N*-acetylaspartate (NAA) peak at 2 ppm (*arrow*) that is much higher than expected for age. Cr2 = phosphocreatine, Cho = choline, Cr = creatine.
D, 2-year-old boy with gradually progressing ataxia and dysarthria, megalencephalic leukoencephalopathy, and subcortical cysts. Coronal T2-weighted MR image shows diffuse abnormal high signal intensity and swelling of white matter and subcortical cyst (*arrow*) in right superior frontal gyrus.

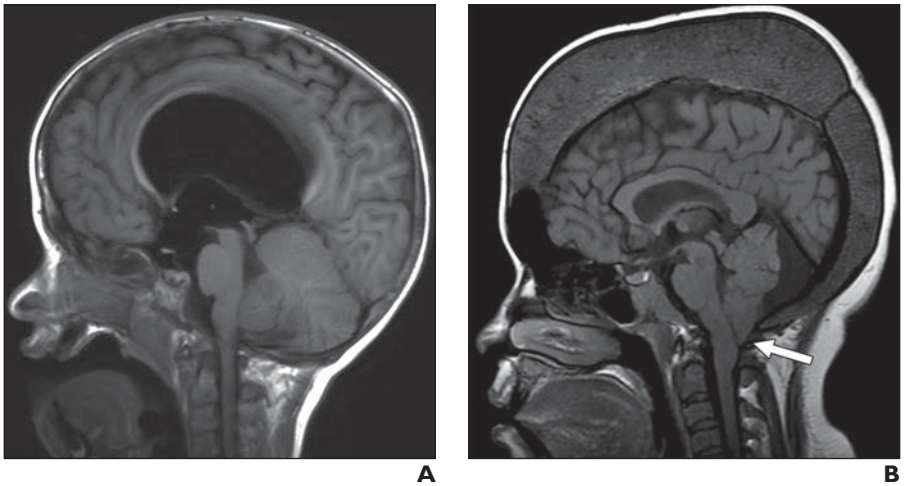

Fig. 10—Osseous abnormalities.
A, 17-year-old girl with thalassemia and long-standing progressive macrocephaly due to extramedullary hematopoiesis. Sagittal T1-weighted MR image shows marked calvarial thickening and secondary cerebellar tonsillar herniation.
B, 6-year-old boy with achondroplasia. Sagittal T1-weighted MR image shows macrocephaly with frontal bossing and supratentorial hydrocephalus with effacement of CSF spaces around foramen magnum (*arrow*).